Bulletin of the Seismological Society of America, Vol. 86, No. 1B, pp. S126–S137, February 1996

Basin Structure Effects on Long-Period Strong Motions in the San Fernando Valley and the Los Angeles Basin from the 1994 Northridge Earthquake and an Aftershock

by Arben Pitarka and Kojiro Irikura

Abstract The strong ground motions recorded within the San Fernando Valley and in the Los Angeles Basin during the 17 January 1994 Northridge earthquake show complex waveforms and complicated patterns of peak acceleration and velocity. This complexity persists even at long periods (1 to 10 sec). We investigate basin structure effects on long-period wave propagation in the San Fernando Valley and in the Los Angeles Basin by the two-dimensional finite-difference modeling of the mainshock and one selected aftershock with $M = 4.1$.

The aftershock ground motion records in the San Fernando Valley and in the Los Angeles Basin can be explained by basin structure effects, assuming a simple point source model. The structural effects and a source model composed of two subevents can explain the most prominent characteristics of the strong-motion waveforms observed during the mainshock at sites south of the epicenter, while such a combination is not enough to explain the large strong motions observed in the north. This result suggests that the rupture propagation effects significantly amplified the ground motions at sites north of the epicenter.

Introduction

Strong motions of the 17 January 1994 Northridge ($M_w = 6.7$) earthquake and its aftershocks were recorded in a wide area from the San Fernando Valley to the Los Angeles Basin. This earthquake generated not only the largest acceleration ever recorded but also complicated patterns of peak acceleration and peak velocity at sites surrounding the source area. Large peak velocities were observed at stations located north of the epicenter, while high peak accelerations were observed at stations located north and south of the epicenter. Large horizontal accelerations in phases following the direct S wave by more than 4 sec were observed at some sites within the Los Angeles Basin. These patterns persist even at low frequencies, less than 1 Hz. Such observations imply that the local site conditions, the source process, and probably the regional geological structure effects all have a role even in the low-frequency range. It is enlightening to analyze such effects by simulating them separately.

First, we investigate basin structure effects in the San Fernando Valley and in the Los Angeles Basin by modeling strong motions recorded during an aftershock with magnitude 4.1, which was located close to the mainshock. We calculate synthetic seismograms from this event using the 2D finite-difference technique proposed by Vidale *et al.* (1985) and assuming a single point source. The basin velocity model we adopted is derived from a previous study (Vidale and Helmberger, 1988), and the structure model below the basins is derived from a 3D tomographic velocity model of the Northridge and Los Angeles areas (Zhao and Kanamori, 1995).

Next, we apply the same approach for modeling strong motions observed during the mainshock. We model the seismic source with two point sources separated in time and in space. This model was derived from previous source process studies, which showed that the faulting process was dominated by two subevents (e.g., Wald and Heaton, 1994). Based on the simulated waveforms at sites in a linear array from the San Fernando Valley to the Los Angeles Basin, the contribution to the long-period waveforms from both effects of local geological structure and the source is analyzed.

Aftershock Simulation

We have simulated the wave propagation in the San Fernando Valley and in the Los Angeles Basin, recorded during the aftershock of 21 January 1994, 18:52:44 ($M = 4.1$). The epicenter of this aftershock was located at 34.30° N, 118.44° W at a depth of 11 km. The focal mechanism determined by the P-wave first-motion data and the moment tensor inversion method is strike, -69; dip, 44; slip, 70°; and the seismic moment, $M_0 = 2.4 \times 10^{22}$ dyne-cm (D.

Zhao, personal comm., 1994). This aftershock was very well recorded at seven stations deployed roughly in a line, passing through the San Fernando Valley and northern part of the Los Angeles Basin. Five of the stations, installed by SCEC (Southern California Earthquake Center), are broadband STS2 instruments, and two of them are forced-balanced accelerometers. Their coordinates are listed in Table 1, and the locations are shown by solid triangles in Figure 1.

By modeling strong ground motions recorded during this aftershock, we intend first to check the validity of the two-dimensional velocity model adopted in this study and secondly to investigate basin effects on long-period wave propagation. Because of the simple source process, the waveforms of this aftershock are affected mainly by path effects. We expect that wave path effects will be similar for the aftershock and the mainshock because their hypocenters are very close to each other.

Table 1
Strong-Motions Station Location Used in the Aftershock Simulation

Station	Latitude	Longitude
BEAR	34.358	−118.396
FIRE	34.309	−118.446
SFYP	34.237	−118.439
NHFS	34.199	−118.398
LA03	34.090	−118.339
WVES	34.005	−118.279
KLVC	33.835	−118.159

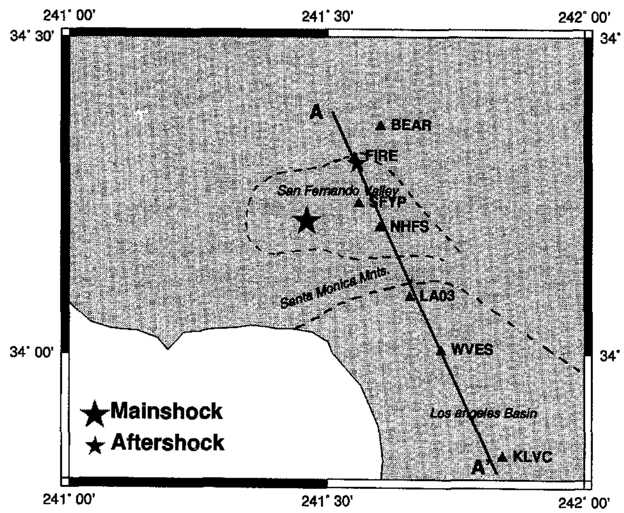

Figure 1. Map of the San Fernando Valley and the Los Angeles regions. The epicenters of the mainshock and the aftershock are marked by filled stars. The filled triangles are the locations of the strong-motion stations used in the aftershock simulation, and the dotted lines represent the basin boundaries. The two-dimensional velocity model used in the aftershock simulation corresponds to the cross section along the profile A-A′.

Velocity Model and Numerical Simulations

The velocity structure (Fig. 2a and Table 2) along the profile passing through the San Fernando Valley and the Los Angeles Basin (which we adopted) is similar to the one proposed by Vidale and Helmberger (1988). Their basins model is based on the stratigraphy, the velocities, and the densities found by Duke *et al.* (1971), while the velocities below the basins were taken from Kanamori and Hadley. Using such a model, they explained the main characteristics of the strong ground motions recorded within the San Fernando Valley and the Los Angeles Basin during the 1971 San Fernando earthquake. For the structure below the basins and the upper crust, we adopted the model recently proposed by Zhao and Kanamori (1995) based on tomography *P*-wave travel-time inversions (Fig. 2b). The *S*-wave velocities are computed assuming $Vp/Vs = 3^{1/2}$, where Vp and Vs are *P*- and *S*-wave velocities, respectively.

For calculating velocity seismograms from a point source, we use the technique proposed by Vidale *et al.* (1985) and Helmberger and Vidale (1988). The *SH* waves are calculated using an elastic finite-difference method (FDM) scheme of second-order accuracy in space (Boore, 1972; Zahradnik and Urban, 1984), and the *P-SV* waves are calculated using an elastic staggered FDM scheme of fourth-order accuracy (Levander, 1988). Absorbing boundary conditions proposed by Stacey (1988) are applied at all boundaries, except the surface where free-surface-stress conditions are imposed. The source box technique proposed by Alterman and Karal (1968) was applied for introducing the seismic energy into the grid.

We simulated the velocity waveforms at frequencies only up to 1 Hz, because FDM is expensive when applied to modeling wave propagation in huge realistic structures. In this study, one reason that the above frequency limitation is justified is that there is not enough detailed knowledge on the geological structure in and around the Los Angeles Basin and in the San Fernando Valley to have confidence in higher-frequency simulations. The second reason is that by modeling aftershock ground motions, we intend to evaluate basin structure effects at low frequencies. This is helpful for distinguishing between the path effects and the source effects observed during the mainshock.

First, we have tested the attenuation effects due to the basin soft sediments by comparing point source *SH* seismograms obtained by using both elastic and anelastic FDM schemes. The technique proposed by Emmerich and Korn (1987) was applied for considering the anelastic attenuation of soils. This technique makes possible a correct inclusion of the attenuation into time domain calculations. But it has the disadvantage of requiring much more memory and computations than the elastic scheme.

We adopted a constant quality factor $Q = 50$ for the basin sediments. Both the elastic and the anelastic scheme were applied for calculating synthetic point source seismo-

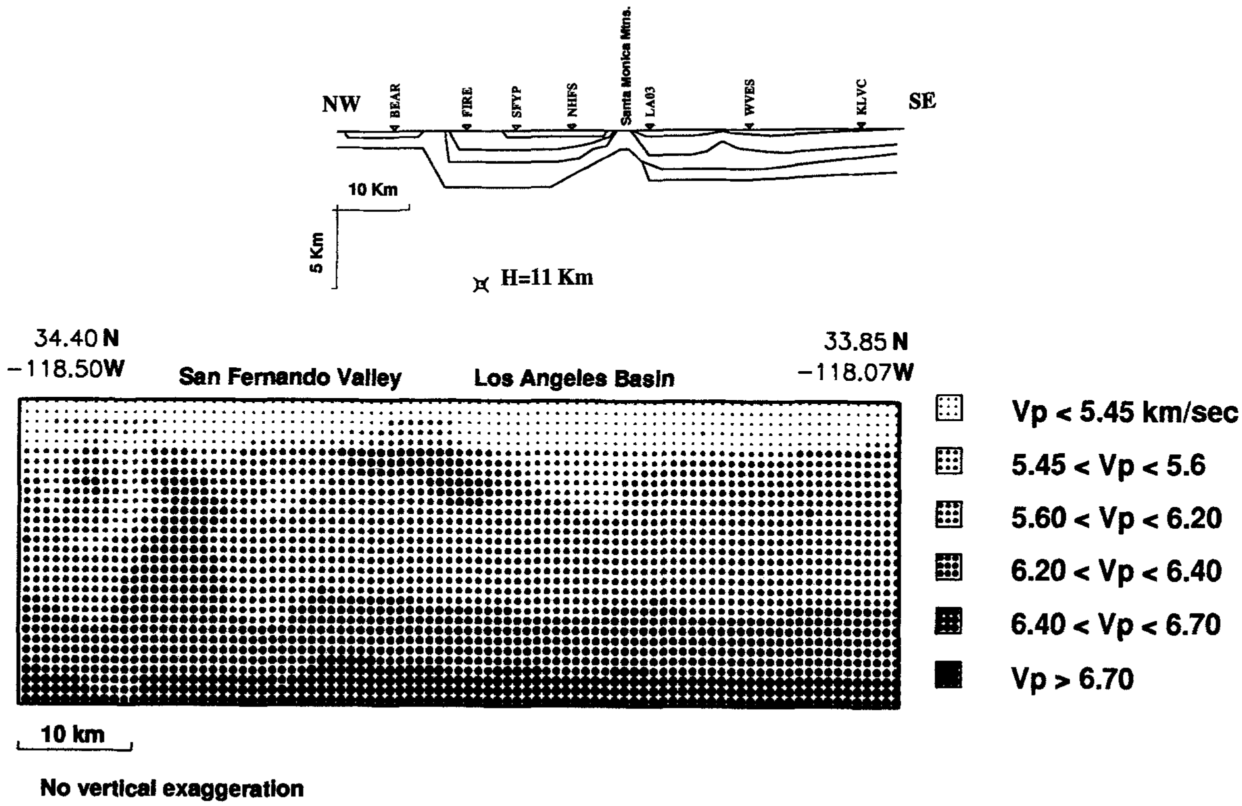

Figure 2. (a) Upper part of the structural cross section of the profile A-A′ and the station locations. The stratigraphy and the velocity model are taken from Vidale and Helmberger (1988). (b) *P*-wave velocity structure along profile A-A′ derived from the 3D velocity structure proposed by Zhao and Kanamori (1995). The velocity intervals are arbitrarily chosen.

Table 2
Velocity Structure for the Cross-Section Shown in Figure 2

P-Wave Velocity (km/sec)	*S*-Wave Velocity (km/sec)	Density (gm/cm^3)
1.4	0.6	1.7
2.0	1.1	1.8
2.5	1.4	1.9
3.1	1.8	2.1
4.3	2.5	2.3

grams at stations shown in Figure 1. The bandpass-filtered synthetics are shown in Figure 3.

The attenuation effect is negligible at sites close to the edges of the basins, while it is significant at sites inside the Los Angeles Basin. Love waves generated at the northern edge of the basin are attenuated while propagating laterally within the soft surface layers. It is important to notice that the amplitude of the body waves one time reflected from the surface is not affected as much, probably because of their relatively short propagation path within the sediments. Despite such effects, for economical reasons, we have performed only elastic finite-difference modeling. The attenuation effects found in this section will be considered in our final interpretations.

The Aftershock Simulation

The simulation of the strong ground motion from the aftershock is shown in Figure 4. We have used a bell-shaped source time function with duration $T_0 = 0.6$ sec and a seismic moment of $M_0 = 1.8 \times 10^{24}$ dyne-cm, which is slightly smaller from that found by Zhao (personal comm., 1994). The three components of the simulated velocity seismograms are compared with those of the recorded ones.

The agreement between the recorded and the synthetic waveforms is in general good. The simulation reproduces some of the most noticeable features of the recorded ground motions. The comparison between the synthetic and the observed seismograms suggests that the surface waves generated at the basin edges and the multiple surface layer reflections gave the main contribution to the observed waveforms. Their possible constructive interference might be the reason for the large amplitude of later phases observed at sites in the Los Angeles Basin and at NHFS in the San Fernando Valley (see Fig. 4).

This simulation raises two problems that concern the

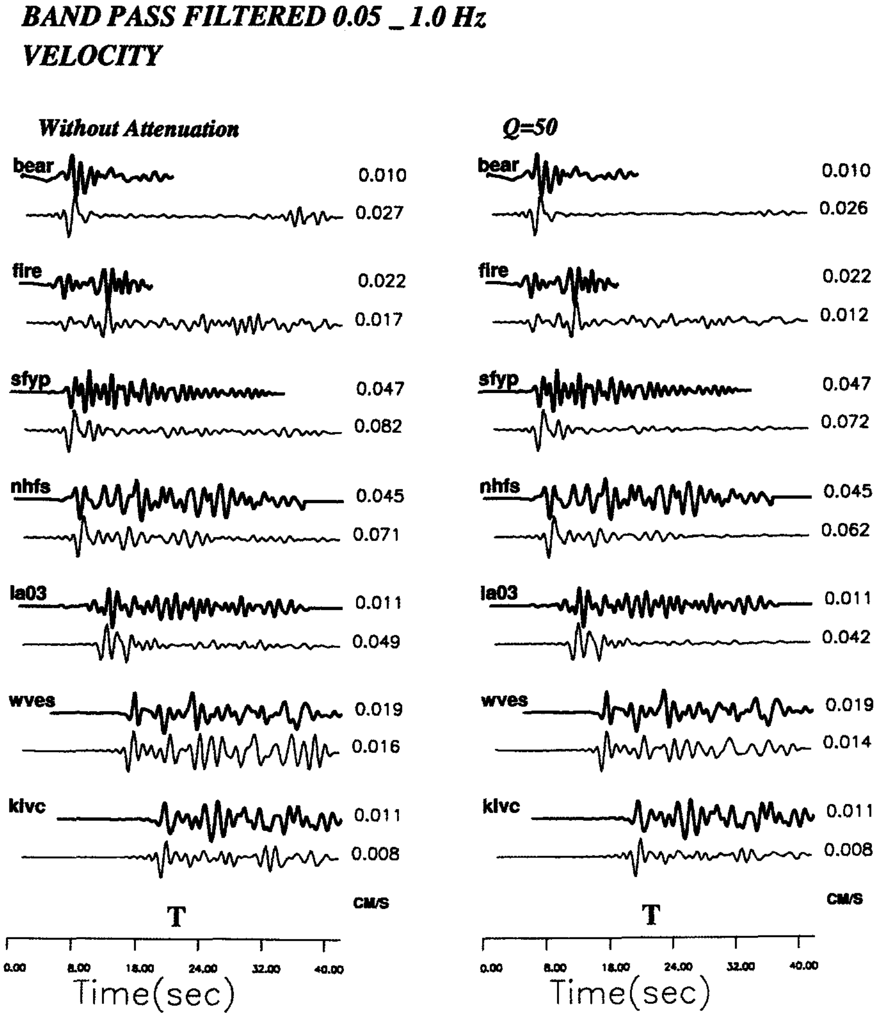

Figure 3. Transverse *SH* component of the recorded and the simulated point source velocity seismograms for the aftershock of 21 January 1994. Left: elastic scheme. Right: anelastic scheme, $Q = 50$. The source time function is a bell-shaped function with time duration $T_0 = 0.8$ sec. The moment scaling and the focal mechanism is discussed in the text. The heavy traces show the data, with the station name and the epicentral distance to the left and the amplitude to the right. The light traces show the synthetic seismograms.

velocity model. First, even though the attenuation is not taken into consideration, the amplitudes of later phases coming after the direct *S* wave in the synthetics at the SFYP station are relatively small compared with those of the recorded ones, in both radial and transverse components. They are mainly secondary surface waves and surface layer multiples that are trapped within the soft layers (e.g., Aki and Larner, 1970; Bard and Bouchon, 1980a, 1980b, 1985; Ohtsuki and Harumi, 1983; Zahradnik and Hron, 1987; Kawase and Aki, 1989). The amplitudes of these waves depend on the geometrical relation between the hypocenter and the basin edge, i.e., the radiation pattern effects from the source, the velocity contrast between the soft basin sediments and the hard rock, and the basin shape (Bard and Bouchon, 1980a, 1980b, 1985; Gaffet and Bouchon, 1991; Yamanaka *et al.,* 1989). An inclined interface between the basin bedrock and the sediments is favorable to multiples with a larger amplitude than direct wave (Helmberger and Vidale, 1988; Frankel and Vidale, 1992; Scott *et al.,* 1994). A smaller slope of the northern edge of the San Fernando Valley, compared with our model, might create multiples with a larger amplitude. Other possibilities, for explaining the large amplitude of later phases in the record at SFYP, are the focusing of the seismic energy inside the valley because of the three-dimensional basin structure effects and the resonant coupling to Rayleigh modes due to the heterogeneity within the basin (Levander and Hill, 1985).

Second, on the synthetic radial component at station LAO3, the amplitude of the later phases is much larger than in the recordings, while in the transverse component, the situation is reversed. As clearly seen in Figure 4, the later phases are mostly Rayleigh waves generated in the San Fer-

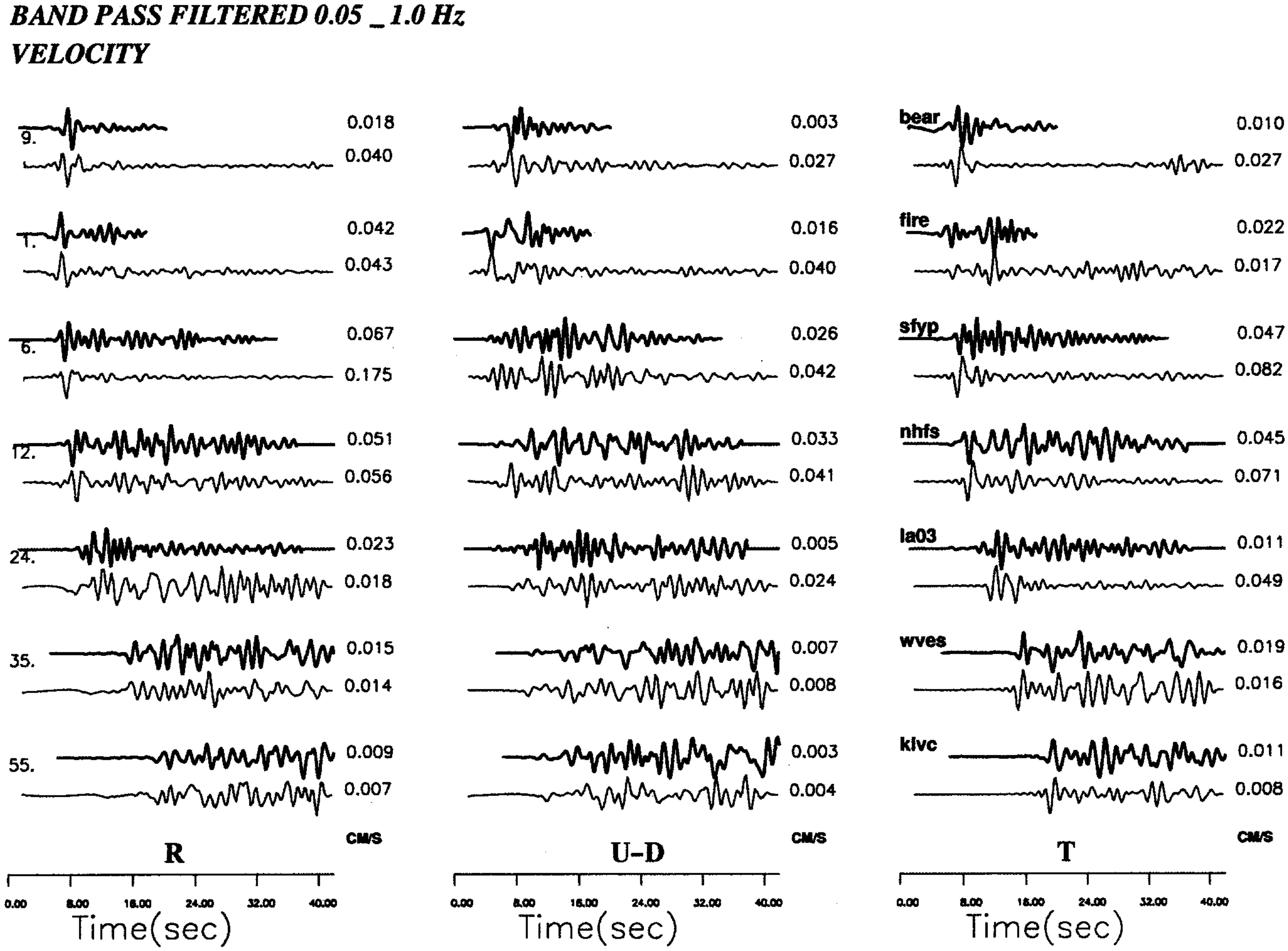

Figure 4. Comparison of filtered velocity recordings with finite-difference velocity seismograms of the 21 January 1994 aftershock, computed for the 2D velocity structure shown in Figure 2. The heavy traces show the recorded seismograms, with the station name and the epicentral distance to the left and the amplitude to the right. The light traces show the synthetic seismograms.

nando Valley, which tunnel across the Santa Monica Mountains. Their amplitude is large compared with the recordings. Such a discrepancy was already observed by Vidale and Helmberger (1988) in their simulation of strong ground motion from the 1971 San Fernando earthquake. They concluded that the three-dimensional effects are at the origin of this problem; the Rayleigh waves generated in San Fernando Valley are refracted into the slower material in the center of the Los Angeles Basin, and their amplitude at sites around station LAO3 might be small. This conclusion is consistent with our simulation; on the synthetic seismograms at stations WVES and KLVC, located at the central part of the basin, the amplitude of the later phases is slightly smaller compared with the recordings.

In Figure 5, we show the peak velocity comparison between the synthetics and the 0.05 to 1.0 Hz bandpass-filtered recordings. The agreement is good, except for the radial component of station SFYP, which is located close to the epicenter. A possible reason for this misfit is that the synthetics at such close stations are very sensitive to the accuracy of the epicentral location. Another reason might be that the finite-difference technique we use does not handle the near-field terms properly at small horizontal distances. Also, the station location very close to the northern edge of the surface basin layer might have affected the abnormal amplification.

It is important to notice the most prominent effects of the two-dimensional velocity structure on the synthetic waveforms shown in Figure 6. In the San Fernando Valley, surface waves generated at the two edges are trapped within the basin. A part of the Rayleigh waves are converted into body waves propagating inside the Santa Monica Mountains and reconverted into surface waves in the Los Angeles Basin. Within the San Fernando Valley, at sites south of the epicenter, the constructive interference between the surface waves and the surface multiples increases the amplitude of later phases.

In the Los Angeles Basin, the phases coming after the

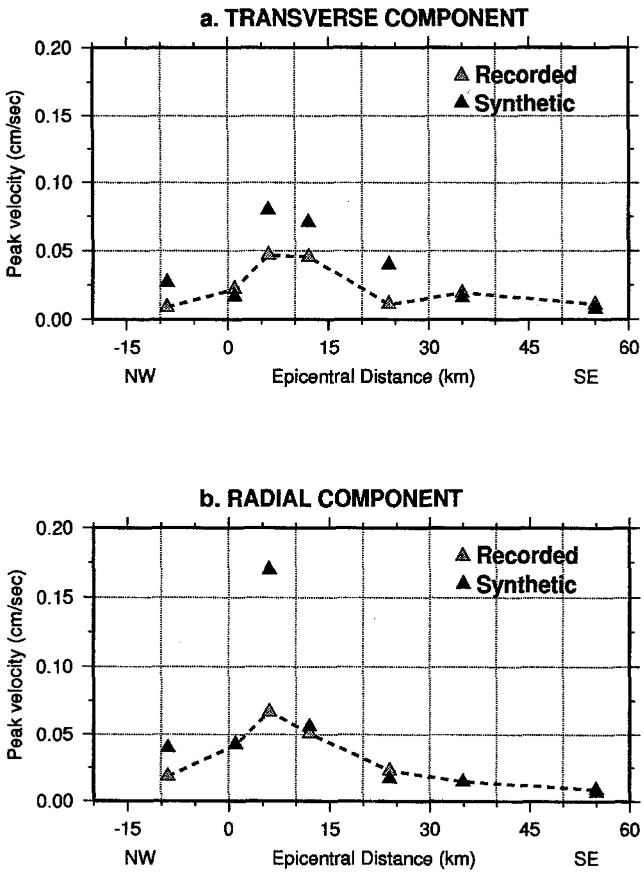

Figure 5. Peak velocity versus distance for the aftershock. The open triangles show the peak velocity of the filtered recordings, and the filled triangles show the peak velocity of the finite-difference simulation: (a) transverse component; (b) radial component.

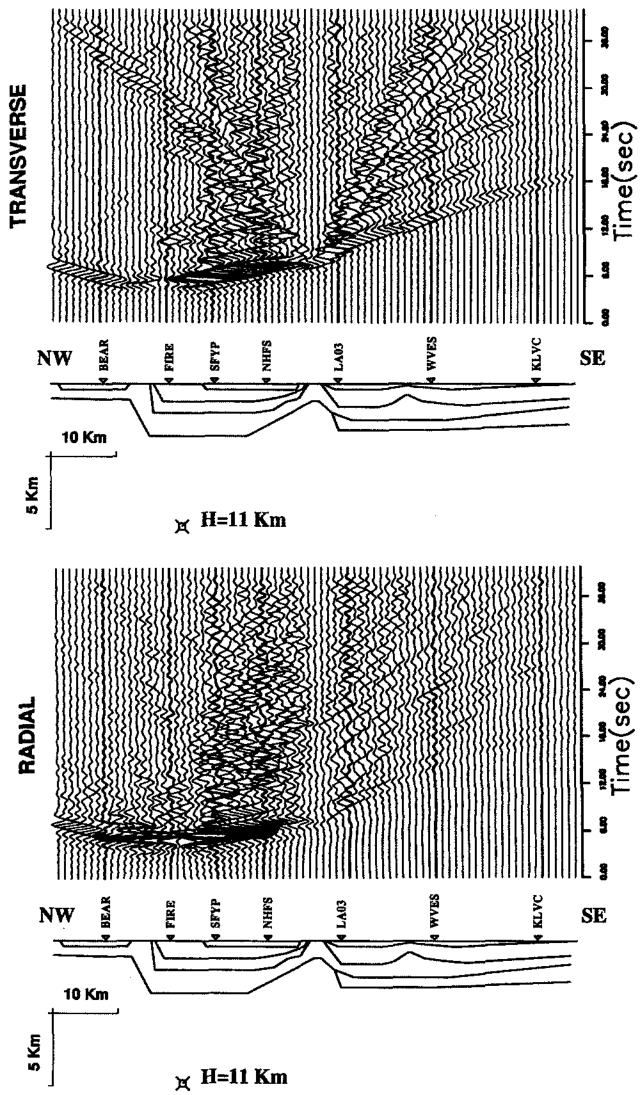

Figure 6. (a) Transverse component of synthetic velocity seismograms calculated across the San Fernando Valley and the Los Angeles Basin. The velocity profile and the location of the stations used in the comparison between the synthetics and the data are shown adjacent to the traces. (b) Radial component of synthetic velocity seismograms calculated across the San Fernando Valley and the Los Angeles Basin. The velocity profile and the location of the stations used in the comparison between the synthetics and the data are shown adjacent to the traces.

direct *S* wave dominate the waveforms. The first two later phases arriving soon after the *S* waves are first and second surface multiple reflections. The difference between their arrival time and that of the direct *S* waves is about 3 sec at stations close to the northern edge and increases up to 5 sec at stations toward the center of the basin. The later phases are surface waves generated at the northern edge of the basin. At stations just above the northern edge of the basin, Love waves have large peak amplitudes. Scott *et al.* (1994) found similar results by calculating synthetic point source *SH* seismograms and using a tomographic *S* velocity model. Their comparison between the synthetic ground motion for the Los Angeles Basin velocity model and that for its simplified flat layer model clearly shows that the increasing amplitude of the surface layer multiples with distance is caused by the dipping edge of the basin.

The relatively good fit between the synthetics and the recordings for the aftershock suggests that the adopted two-dimensional velocity structure is useful for predicting low-frequency local geology effects. The simulation shows that for an earthquake located in the Northridge region, the amplifications due to the basin structure are expected to be maximum at sites close to the edges of the San Fernando Valley and along the northern edge of the Los Angeles Basin.

Main Shock Simulation

Source Parameters

Source modeling with empirical Green's functions and waveform inversions (Li and Toksoz, 1994; Dreger, 1994;

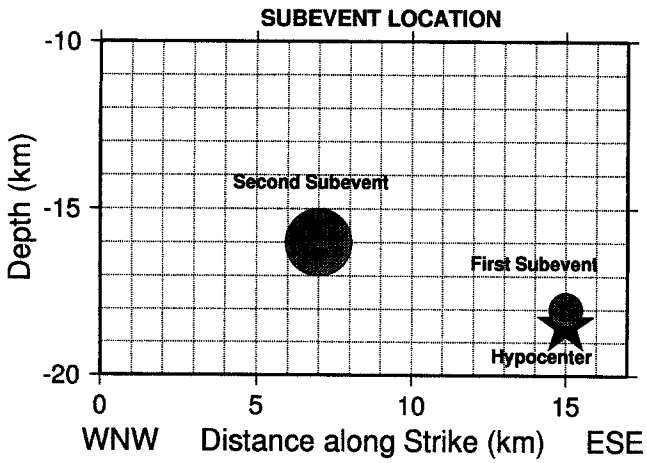

Figure 7. Subevent location in the fault plane. The filled star shows the hypocenter location of the 1994 Northridge earthquake. Shadowed circles show the subevent locations. The moment scaling is explained in the text.

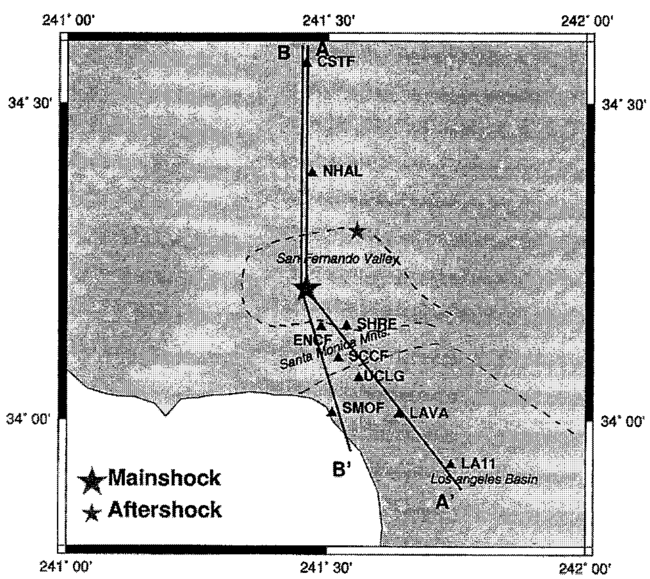

Figure 8. Map of Northridge and Los Angeles regions. The epicenters of the mainshock and the aftershock are marked by filled stars. The filled triangles are the locations of the stations used in the simulation, and the dotted lines represent the basin boundaries. The two-dimensional velocity models used in the mainshock simulations correspond to the cross sections along the profiles A-A′ and B-B′.

Song *et al.,* 1994; Wald and Heaton, 1994; Thio and Kanamori, 1994) show that the mainshock is composed of two or more subevents and that the rupture propagated northward and updip. Li and Toksoz (1994) found that the rupture started with a relatively small subevent and released most of the energy during the second subevent. In terms of energy released, Song *et al.* (1994) found an average source depth of 15 km, which is close to that found by Thio and Kanamori (1994). Studies of the source process indicate that a single fault plane ruptured (Wald and Heaton, 1994; Song *et al.,* 1994). A dislocation model determined from strong motions records near the hypocenter (Wald and Heaton, 1994) shows that the biggest amount of slip is northwest of the hypocenter at depths between 15 and 18 km, which is consistent with the subevents found by Thio and Kanamori (1994) from the waveform inversion of teleseismic body waves. Their solution shows the first subevent at 19 km, the second subevent at 17 km, and the third smaller subevent at about 13 km. They found a 2-sec time difference between the first two subevents, while Li and Toksoz (1994) found 2.5 up to 3 sec.

An along strike subevent separation of about 8 km is consistent with the observation that the two main first arrivals are separated in time by 4 to 5 sec at sites in the south and by less than 3 sec in the north. By assuming a constant rupture velocity of 2.7 km/sec, the time interval between the two events should be around 3 sec.

Based on the above information, we model the seismic source by two point sources located at different depths, as shown in Figure 7, and assume a 3.0-sec time interval between the two subevents. Their location corresponds to the asperities found by Wald and Heaton (1994). Such a source model does not include rupture propagation effects; conse-

Table 3
Strong Motion Stations Used in the Mainshock Simulation

Station	Latitude	Longitude
CSTF	34.564	−118.642
NHAL	34.390	−118.530
SHRF	34.151	−118.463
SCCF	34.100	−118.478
UCLG	34.068	−118.439
LABA	34.009	−118.361
LA11	33.929	−118.260
ENCF	34.149	−118.512
SMOF	34.011	−118.490

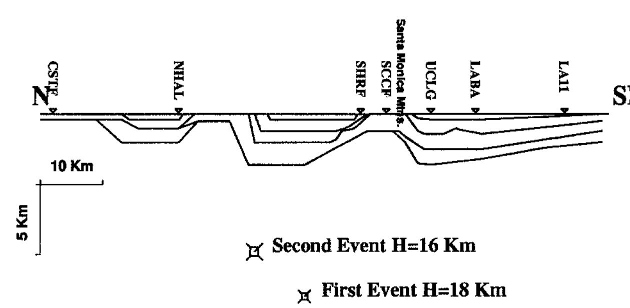

Figure 9. Upper part of the structural cross section of the profile A-A′ (shown in Fig. 8) and the station locations. The stratigraphy and the velocity model are taken from Vidale and Helmberger (1988). The velocity model below the basins is shown in Figure 2b.

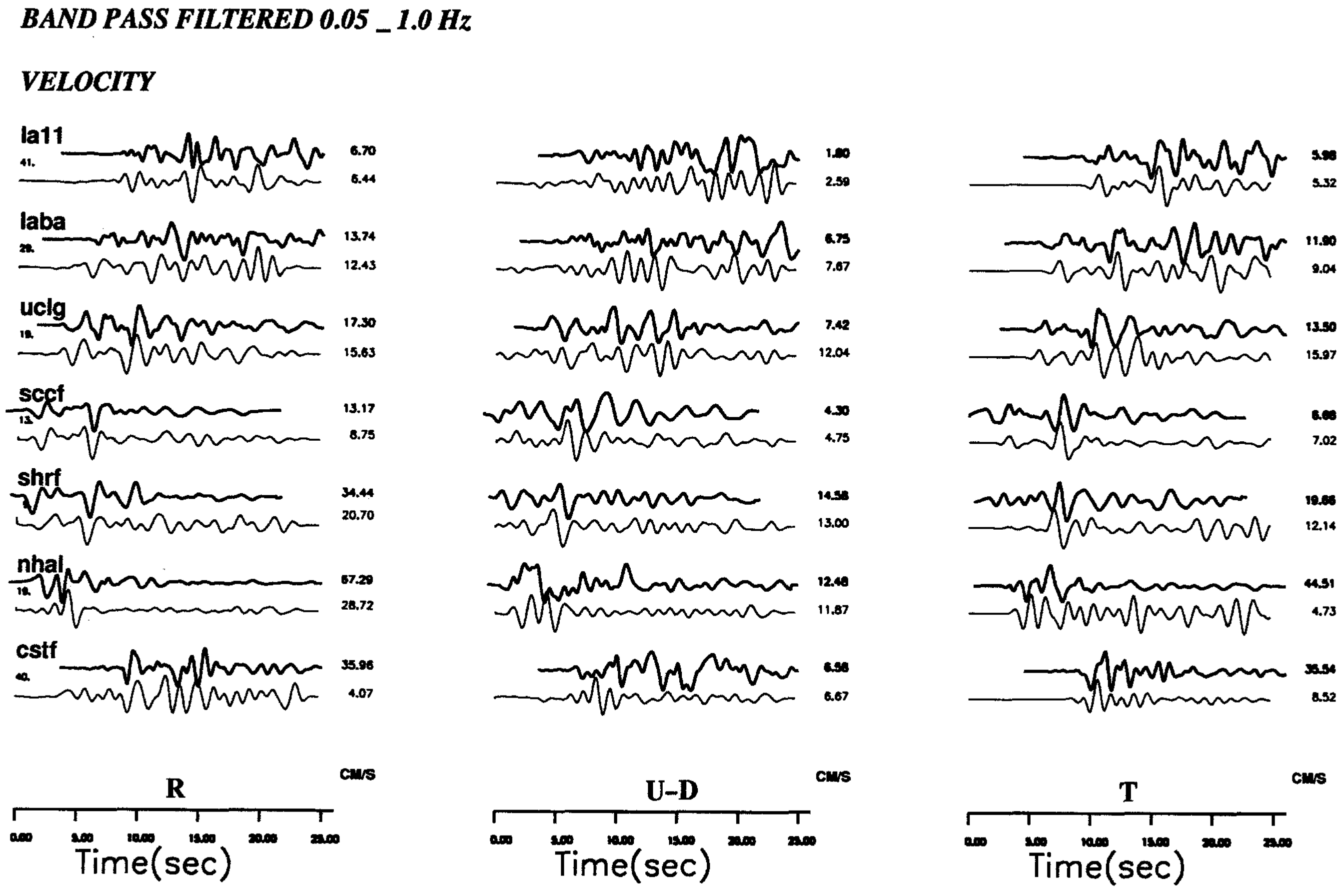

Figure 10. Comparison of filtered velocity records with finite-difference velocity seismograms of the 17 January 1994 Northridge earthquake, computed for the 2D velocity structure shown in Figure 9. The heavy traces show the data, with the station name and the epicentral distance to the left and the amplitude to the right. The light traces show the synthetic seismograms. The location of the two subevents is shown in Figure 7. See text for source time function model.

quently, it is probably most applicable for explaining strong motion at sites located south of the epicenter where the rupture propagation effect is not significant, as shown by previous studies (Wald and Heaton, 1994). We use the same bell-shaped source time function with a time duration of 1.2 sec and the same focal mechanism for both subevents. A seismic moment ratio between the first and the second subevent of 0.5 and the focal mechanism found by Thio and Kanamori (1994) (134/42/114 [strike/dip/slip]) were used in the forward strong-motion modeling.

Numerical Results

The same technique as the one used for the aftershock was applied for calculating velocity seismograms at stations aligned along the A-A′ profile (Fig. 8) where the mainshock ground motions were recorded. We use strong-motion accelerograms from the California Division of Mines and Geology (Shakal *et al.,* 1994), the U.S. Geological Survey (Porcella *et al.,* 1994), and the Los Angeles Department of Power and Water (Wald, personal commun.) (see Table 3).

The recorded accelerograms were first integrated to velocity and then bandpass-filtered (0.05 to 10.0 sec). The upper part of the velocity structure corresponding to the A-A′ profile is shown in Figure 9. The result of the simulation is shown in Figure 10. Since there is no absolute timing for the data, the match in timing is done arbitrarily following the first clear pulse seen in the transverse component.

We find that the two point sources separated in space and time and with the same focal mechanism can predict most of the long-period ground motions recorded at sites within the San Fernando Valley and in the Los Angeles Basin. The fit between the recordings and the synthetics is good at almost all the stations to the south, especially at the rock site, the SCCF station. This result proves the validity of our source model. However, at two stations to the north, NHAL and CSTF, there is a great difference not only in the waveforms but also in the peak amplitudes. At these stations, the peak amplitude of the data is almost four times greater than the one obtained by the simulations (Fig. 11). Such differences cannot be explained by inaccuracies in the velocity model, because the aftershock simulation showed its validity for evaluating site effects even at northern sites. We attribute them to the fact that, comparing with those to the south of epicenter, the recorded motions to the north of the rupture are more sensitive to the details of the source process. Wald and Heaton (1994) found a strong effect of the source radiation (radiation pattern and rupture directivity) at stations located north of the hypocenter.

A seismic moment ratio of 0.5 between the first and the second event produced the best fit between the recordings and the simulations. The total seismic moment needed to fit the bandpass-filtered seismograms (0.05 to 1.0 Hz) is smaller than the amount found for this earthquake by other researchers. This is because the velocity records used in the modeling do not have much of a signal above a 3-sec period to constrain the long-period motions. The assumed source time function with duration 1.2 sec, adopted for fitting the velocity records at periods around 1 to 2 sec, is too short to replicate the real Northridge source, which probably lasted more than 5 sec.

Our source model predicts the two distinct arrivals and the large amplitudes of later phases observed at sites located south and southeast of the epicenter. It is interesting from the strong ground motion prediction point of view to clarify the origin of the large-amplitude later phases recorded at stations in the Los Angeles Basin, close to the northern edge. Li and Toksoz (1994) suggest that this may be caused by the mainshock subevents having different focal mechanisms. However, Thio and Kanamori (1994) found only slight differences between the focal mechanisms of the first two subevents of the mainshock. Without ruling out the source contribution, Wald and Heaton (1994) favor that this effect comes from the site conditions since several aftershocks recorded along the northern edge of the Los Angeles Basin show later arrivals as well.

Based on the above simulation, we attribute the waveform complexity observed at stations located north of the Los Angeles Basin (SMOF, UCLG, LABA) to a possible constructive contribution from both site effects and source processes. At these stations, the direct S wave corresponding to the second biggest subevent arrives about 4 to 5 sec after the direct S wave corresponding to the first subevent. This is close to the arrival time found for the first surface layer multiple or surface wave associated to the first subevent. We have considered separately the local site effects on the ground motion from the first small subevent and the effect from the second subevent. In Figure 12, for stations south of the epicenter, we display the observed records (top trace) and the synthetic records (second trace) along with the separate contributions to the synthetic records from the first subevent (third trace) and the second subevent (bottom trace).

From this figure, it can be seen that at sites close to the northern edge of the Los Angeles Basin (e.g., LA11, LABA), a double-event source process combined with local site effects might cause large strong ground motions.

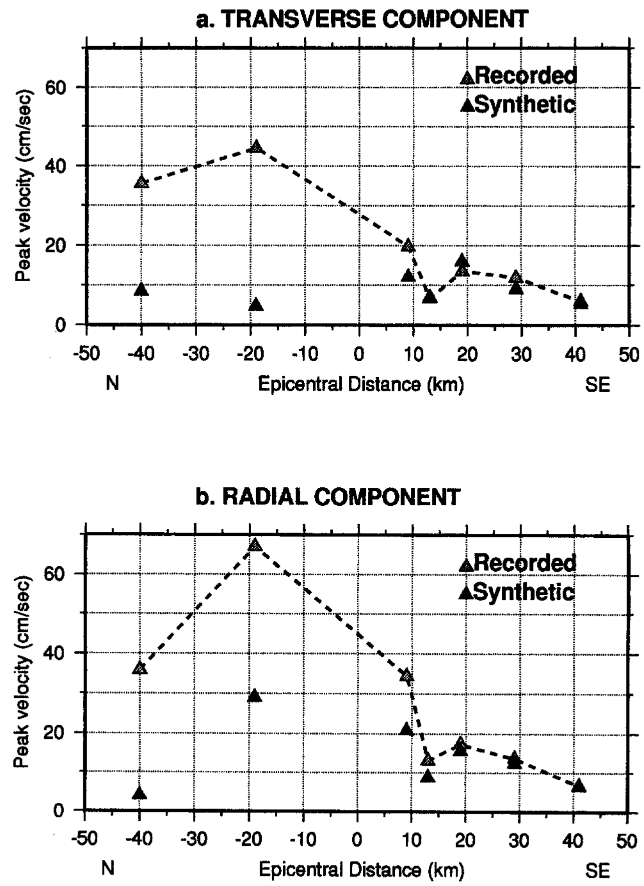

Figure 11. Peak velocity versus distance for the mainshock. The open triangles show the peak velocity of the filtered data, and the filled triangles show the peak velocity of the finite-difference simulation: (a) transverse component; (b) radial component.

We performed another simulation along the profile B-B′ shown in Figure 8. This profile passes through the Santa Monica site (SMOF) where large-amplitude later phases were recorded. Our intention was to find an explanation for the long-period waveforms observed at SMOF.

We used the same source model as we did for the previous mainshock simulation. Again, the synthetics at the northern station (NHAL) have much smaller amplitudes as compared with the observed records (see Fig. 13). The synthetic waveforms at SMOF show that the large-amplitude later phases are mainly secondary surface waves generated at the northern edge of the Los Angeles Basin. Their arrival time predicted by the simple velocity model we use is slightly greater than the observed one. The generation of those surface waves is probably controlled either by a three-dimensional large-scale structure or by a shallow microbasin structure with the northern edge close to SMOF.

A comparison between two- and three-dimensional wave propagation simulations may better clarify the site effects at Santa Monica and the factors controlling the amplitude of the surface waves generated close to this site.

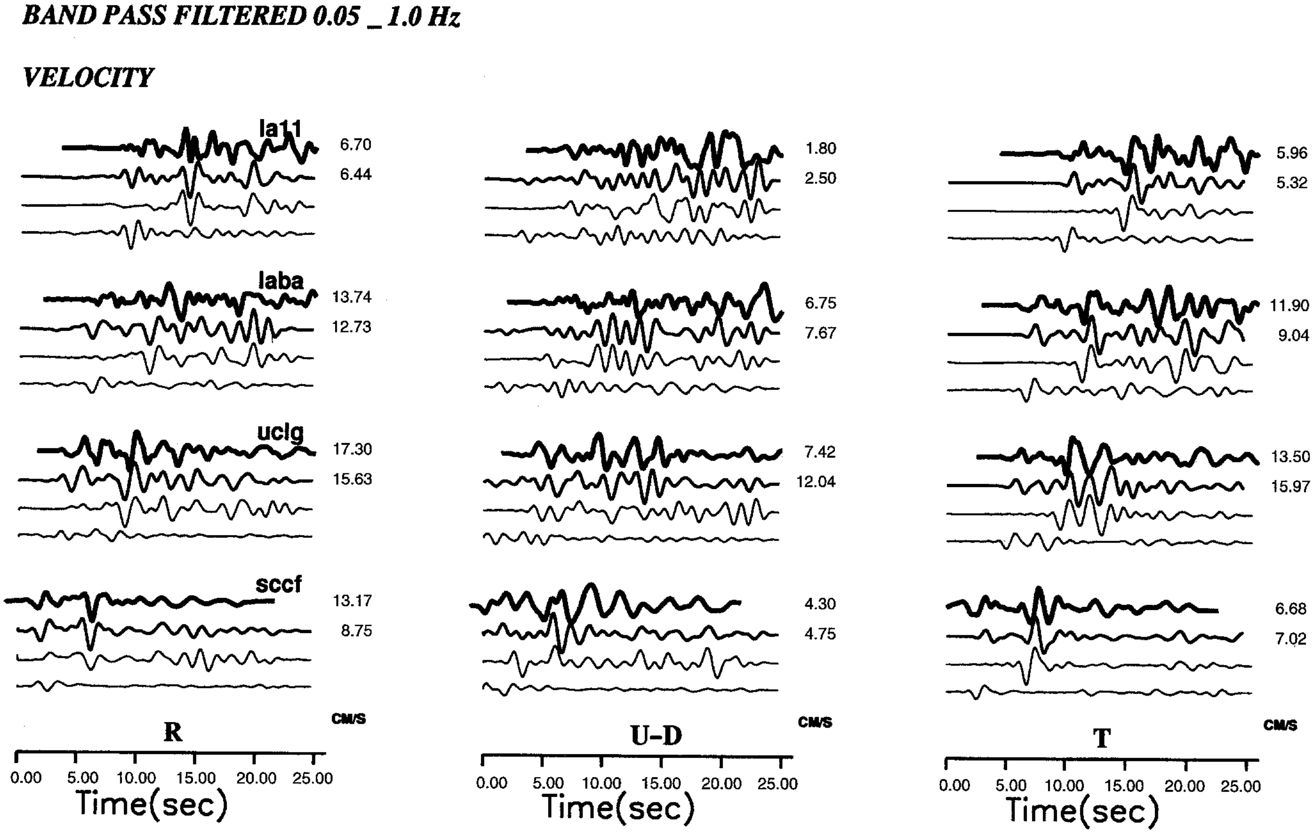

Figure 12. Comparison of data (heavy top trace) and synthetics (second trace) with contributions to the synthetics from second subevent (third trace) and first subevent (forth trace) for stations located along the profile A-A′.

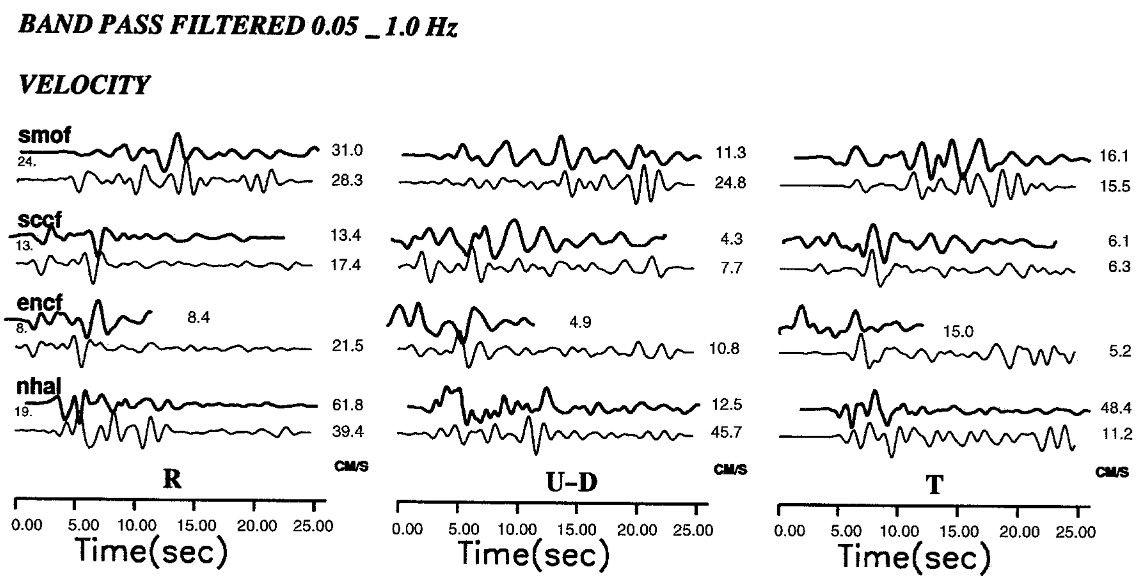

Figure 13. Comparison of filtered velocity data with finite-difference velocity seismograms of the 17 January 1994 Northridge earthquake, computed for the 2D velocity structure corresponding to the profile B-B′ shown in Figure 8. The heavy traces show the data, with the station name and the epicentral distance to the left and the amplitude to the right. The light traces show the synthetic seismograms. The source model used in the simulation is discussed in the text.

Conclusions

Two-dimensional finite-difference modeling, based on a heterogeneous velocity structure and a source model consisting of a double-couple point source, can reproduce the most prominent characteristics of the long-period (1 to 10 sec) strong ground motions recorded in the southern part of the San Fernando Valley and in the Los Angeles Basin during an aftershock of the January 1994 Northridge earthquake. We found that both the valley and the basin generate secondary waves that dominate the later arrivals. The modeling of the mainshock using two double-couple point sources separated in space and in time, with the same focal mechanism and with a seismic moment ratio of 0.5, indicates significant basin effects that can be identified in the observed strong ground motions.

At sites within the San Fernando Valley, the ground motions have been significantly affected by the surface waves excited at the edges of the valley. Basin effects and the multiple event source process have contributed to the amplification of the second main arrival observed at sites close to the northern edge of the Los Angeles Basin. A three-dimensional or more accurate two-dimensional velocity structure may better explain some small inconsistencies between the recordings and the synthetics at sites where local effects seem to be more complex, such as in Santa Monica.

The large difference between the peak amplitudes of the mainshock recordings and the synthetics at sites north of the epicenter, while a good fit between the synthetic and the recorded waveforms is obtained to the south, suggests that at sites north of the epicenter, the rupture propagation effect dominates over site effects.

Acknowledgments

We would like to thank Adam Edelman for kindly providing us with the strong-motion data of the aftershock; David Wald for providing us with the January 1994 Northridge earthquake strong-motion data recorded at the SHRF, ENCF, and SCCF stations; and Dapeng Zhao for preparing the *P*-wave velocity models of the upper crust. We are grateful to F. J. Sanchez-Sesma, H. Takenaka, and D. Suetsugu for their valuable discussions. We greatly appreciate the constructive review by Keith L. McLaughlin and an anonymous reviewer. This work was in part supported by the Grant-in-Aid for Scientific Research No. 05302069 from the Ministry of Education, Science and Culture, Japan, and the Kajima Foundation's Research Grant.

References

Aki, K. and K. L. Larner (1970). Surface motion of a layered medium having an irregular interface due to incident plane SH waves, *J. Geophys. Res.* **75,** 933–954.

Alterman, Z. and F. C. Karal (1968). Propagation of elastic waves in layered media by finite-difference methods, *Bull. Seism. Soc. Am.* **58,** 367–398.

Bard, P. Y. and M. Bouchon (1980a). The seismic response of sediment-filled valleys. Part 1. The case of incident SH waves, *Bull. Seism. Soc. Am.* **70,** 1263–1286.

Bard, P. Y. and M. Bouchon (1980b). The seismic response of sediment-filled valleys. Part 2. The case of incident P and SV waves, *Bull. Seism. Soc. Am.* **70,** 1921–1941.

Bard, P. Y. and M. Bouchon (1985). The two-dimensional resonance of sediment-filled valleys, *Bull. Seism. Soc. Am.* **75,** 519–542.

Boore, D. M. (1972). Finite-difference methods for seismic waves, in *Methods in Computational Physics,* B. A. Bolt (Editor), Vol. 11, Academic Press, New York, 1–37.

Dreger, D. S. (1994). Empirical Green's function study of the January 17, 1994 Northridge mainshock (Mw = 6.7), submitted to *Geophys. Res. Lett.*

Duke, C. M., J. A. Johnson, Y. Kharraz, K. W. Campbell, and N. A. Malpiede (1971). Subsurface site conditions and geology in the San Fernando earthquake area, UCLA-ENG-7206, School of Engineering, UCLA, Los Angeles, California.

Emmerich, H. and M. Korn (1987). Incorporation of attenuation into time-domain computations of seismic wavefields, *Geophysics* **52,** 1252–1264.

Frankel A. and J. Vidale (1992). A three-dimensional simulation of seismic waves in the Santa Clara Valley, California, from a Loma Prieta aftershock, *Bull. Seism. Soc. Am.* **82,** 2045–2074.

Gaffet S. and M. Bouchon (1991). Source location and valley shape effects on the P-SV near displacement field using boundary integral equation-discrete wave number representation, *Geophys. J. Int.* **106,** 341–355.

Helmberger, D. V. and J. E. Vidale (1988). Modeling strong motions produced by earthquakes with two-dimensional numerical codes, *Bull. Seism. Soc. Am.* **78,** 109–121.

Kawase, H. and K. Aki (1989). A study on the response of a soft basin for incident S, P and Rayleigh waves with special reference to the long duration observed in Mexico city, *Bull. Seism. Soc. Am.* **79,** 1361–1382.

Levander, A. R. (1988). Fourth-order finite-difference P-SV seismograms, *Geophysics* **53,** 1425–1436.

Levander, A. R. and N. R. Hill (1985). P-SV resonances in irregular low-velocity surface layers, *Bull. Seism. Soc. Am.* **75,** 847–864.

Li, Y. and M. N. Toksoz, (1994). Empirical Green's function analysis of source time functions for the mainshock and large aftershocks of the January 17, 1994 Northridge earthquake sequence, 89th SSA Meeting, Pasadena, California, 1994.

Ohtsuki, A. and K. Harumi (1983). Effect of topographies and subsurface inhomogeneities on seismic SV waves, *Earthquake Eng. Struct. Dyn.* **11,** 444–461.

Porcella, R. L., E. C. Etheredge, R. P. Maley, and A. V. Acosta (1994). Accelerograms recorded at USGS national strong-motion network stations during the Ms = 6.6 Northridge, California earthquake of January 17, 1994, *U.S.G.S. Open-File Report 94–141.*

Scott, J. S., E. Hauksson, F. Vernon, and A. Edelman (1994). Los Angeles basin ground motion estimation for aftershocks of the 1994 Northridge Earthquake from a tomographic velocity model, 89th SSA Meeting, Pasadena, California, 1994.

Shakal, A., M. Huang, R. Darragh, T. Cao, R. Sherburne, P. Malhotra, C. Cramer, R. Sydnor, V. Graizer, G. Maldonado, C. Peterson, and J. Wampole (1994). CSMIP strong motion records from the Northridge, California earthquake of 17 January, 1994. Report No. OSMS 94-07, California Strong Motion Instrumentation Program.

Song, X., L. Jones, and D. V. Helmberger (1994). Source characteristics of the January 17, 1994 Northridge California earthquake from regional broadband modeling, 89th SSA meeting, Pasadena, California, 1994.

Stacey, R. (1988). Improved transparent boundary formulations for the elastic-wave equation, *Bull. Seism. Soc. Am.* **78,** 2089–2097.

Thio, H. and H. Kanamori (1994). Source complexity of the 1994 Northridge earthquake, 89th SSA meeting, Pasadena, California, 1994.

Vidale, J. E. and D. V. Helmberger (1987). Path effects in strong motion seismology, in *Methods of Computational Physics,* Vol. 11, Bruce Bolt (Editor) (entitled Seismic Strong Motion Synthetics).

Vidale, J. E. and D. V. Helmberger (1988). Elastic finite-difference modeling of the 1971 San Fernando, California earthquake, *Bull. Seism. Soc. Am.* **78,** 122–141.

Vidale, J. E., D. V. Helmberger, and R. W. Clayton (1985). Finite-difference seismograms for SH waves, *Bull. Seism. Soc. Am.* **75,** 1765–1782.

Wald, J. D. and T. H. Heaton (1994). A dislocation model of the 1994 Northridge, California, earthquake determined from strong ground motions, *U.S.G.S. Open-File Report 94–278.*

Yamanaka, H., K. Seo, and T. Samano (1989). Effects of sedimentary layers on surface-wave propagation, *Bull. Seism. Soc. Am.* **79,** 631–644.

Zahradnik, J. and L. Urban (1984). Effect of a simple mountain range on underground seismic motion, *Geophys. J. R. Astr. Soc.* **79,** 167–183.

Zahradnik, J. and F. Hron (1987). Seismic ground motion of sedimentary valleys: example La Molina, Lima, Peru, *J. Geophys.* **62,** 31–37.

Zhao, D. and H. Kanamori (1995). The 1994 Northridge earthquake: 3-D crustal structure in the rupture zone and its relation to the aftershock locations and mechanisms, *Geophys. Res. Lett.* **22,** no. 7, 763–766.

Disaster Prevention Research Institute
Kyoto University
Gokasho, Uji
Kyoto 611, Japan
(A.P., K.I.)

Manuscript received 1 January 1995.